Precision Engineering xxx (2015) xxx–xxx

Contents lists available at ScienceDirect

Precision Engineering

journal homepage: www.elsevier.com/locate/precision

A new methodology to design multi-sensor networks for distributed large-volume metrology systems based on triangulation

D. Maisano*, L. Mastrogiacomo

Politecnico di Torino (DIGEP), Torino 10129, Italy

ARTICLE INFO

Article history:
Received 23 March 2015
Received in revised form 29 May 2015
Accepted 1 July 2015
Available online xxx

Keywords:
Large-volume metrology
Distributed measuring system
Multi-sensor network
Triangulation
Network design
Network density

ABSTRACT

Distributed Large-Volume Metrology (LVM) systems are mainly used for industrial applications concerning assembly and dimensional verification of large-sized objects. These systems generally consist of a set of network devices, distributed around the measurement volume, and some targets to be localized, in contact with the measured object's surface or mounted on a hand-held probe for measuring the points of interest. Target localization is carried out through several approaches, which use angular and/or distance measurements by network devices.

This paper presents a new methodology to support the design of networks of devices, for distributed LVM systems based on triangulation (i.e., systems in which network devices perform angular measurements only). It is assumed that these systems use multi-sensor networks including two typologies of devices: some are accurate but expensive and other ones are less accurate but cheaper. The goal of the methodology is establishing a link between the following parameters: (i) density of network devices, (ii) mix between the two typologies of network devices, (iii) measurement uncertainty, and (iv) cost. The methodology allows to estimate the most appropriate density and mix between the two typologies of network devices, so that the distributed LVM system is conforming with the required measurement uncertainty and cost.

The methodology relies on a large number of simulated experiments, defined and implemented using a dedicated routine; feasibility and practicality is tested by preliminary experiments on a multi-sensor photogrammetric system, developed at Politecnico di Torino—DIGEP.

© 2015 Elsevier Inc. All rights reserved.

1. Introduction

The use of distributed systems for applications in the field of Large-Volume Metrology (LVM) is more and more diffused and consolidated [1]. Typical industrial applications concern assembly and dimensional verification of large-sized mechanical components, in which levels of accuracy of several tenths of millimetre are tolerated [2,3]. The reason behind the diffusion of distributed LVM systems is simple: arranging a portable measuring system around the object to be measured is often more practical than the *vice versa* [4,5].

In general, distributed LVM systems consist of: (i) a set of *network devices*, distributed around the object to be measured, (ii) some *targets* to be localized, generally in contact with the measured object's surface, or mounted on a hand-held probe for measuring the points of interest, and (iii) a centralized *data processing unit* (DPU), which receives local measurement data from network devices.

The localization of targets is carried out through three possible approaches:

- *Triangulation*, using the angles subtended by targets, with respect to network devices;
- *Multilateration*, using the distances between targets and network devices;
- *Hybrid techniques*, based on the combined use of angles and distances between targets and network devices.

In this paper we deal exclusively with distributed LVM systems based on triangulation; Fig. 1 provides a schematic representation of these systems: each *i*th network device (D_i) is associated with a local coordinate system $o_i x_i y_i z_i$ and is able to perform local angular measurements with respect to a target *P*; the aim of the measurement is localizing *P*, determining its spatial coordinates in the global Cartesian coordinate system *OXYZ*. In Fig. 1, four network devices (i.e., D_1 to D_4) are involved in the measurement, as it

* Corresponding author. Tel.: +39 0110907281.
E-mail address: domenico.maisano@polito.it (D. Maisano).

http://dx.doi.org/10.1016/j.precisioneng.2015.07.001
0141-6359/© 2015 Elsevier Inc. All rights reserved.

Please cite this article in press as: Maisano D, Mastrogiacomo L. A new methodology to design multi-sensor networks for distributed large-volume metrology systems based on triangulation. Precis Eng (2015), http://dx.doi.org/10.1016/j.precisioneng.2015.07.001

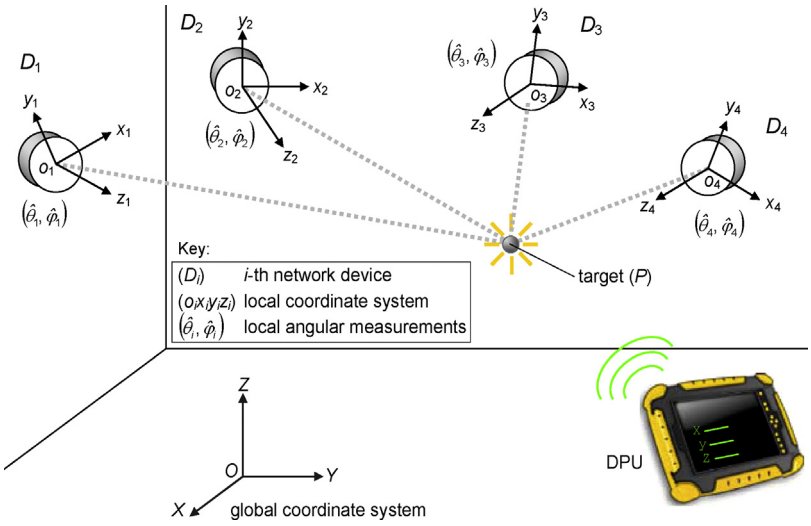

Fig. 1. Schematic representation of a generic distributed LVM system, based on triangulation.

is assumed that they all include P in their range of measurement. In general, the number of devices involved in the localization of a target depends on their mutual positioning/orientation and range of measurement. Each ith network device measures two angles, i.e., θ_i and φ_i, described in Section 2.

Network devices may differ in technology, measurement uncertainty, range of measurement and cost. For example, optical theodolites have uncertainty on angular measurements of a few hundredths of a degree, range of measurement of several tens of meters (with some constraints regarding angles) and cost of a few thousand €; the relatively recent rotary-automatic laser theodolites (R-LATs) have uncertainty on angular measurements of a few thousandths of a degree [6], range of measurement of about 20 m (with some constraints regarding angles) and cost around 50,000€; data related to photogrammetric cameras may fluctuate significantly, depending on their technical/metrological features, such as pixel resolution and frame rate.

When designing a network of devices for a distributed LVM system, two of the most important factors to consider are:

- *network density* (i.e., number of network devices per surface unit), since the uncertainty in target localization tends to decrease with the number of devices, which can "see" the target [7];
- *uncertainty of network devices* in measuring the angles subtended by targets. In general, the more technologically advanced and expensive the network devices, the lower their uncertainty in local angular measurements and, hence, that in target localization.

These factors could be both optimized by using dense networks of very accurate[1] devices, although this solution may result in high cost, in contrast to budget sustainability. A reasonable compromise to achieve good results, while limiting cost, is using multi-sensor[2] networks, which combine: (i) a relatively large number of not very accurate but cheap devices, for obtaining a good coverage of the measurement volume, and (ii) a relatively low number of accurate but expensive devices, for reducing the uncertainty in target localization.

Unfortunately, defining the optimal network density and mix between accurate and less-accurate devices is a difficult task, due to the complexity of the target localization problem and the fact that it can be influenced by several parameters related to network devices (e.g., range of measurement; uncertainty in angular measurement; uncertainty in their location/orientation, due to the calibration process, etc.) [5].

The aim of this paper is introducing a new supporting methodology to design multi-sensor networks for distributed LVM systems based on triangulation, assuming that these networks include two typologies of devices: some are accurate but expensive and other ones are less accurate but cheaper. The goal of the proposed methodology is establishing a link between four parameters: density of network devices (δ), percentage of accurate devices (p_A), measurement uncertainty, and cost. This will be done through a large number of simulated experiments, in which the former two parameters (δ and p_A) are varied and their influence on the latter two parameters is analyzed. In these simulated experiments, target localization is modelled through a consolidated mathematical model, which can be adapted to multi-sensor networks. In practical terms, the proposed methodology allows to estimate the optimal δ and p_A, so that the whole system is conforming with the required measurement uncertainty and cost.

The remainder of this paper is organized into three sections. Section 2 provides some basic concepts concerning the problem of the localization by triangulation and the mathematical model, which is used in the proposed methodology. Section 3 is divided into three parts: the first one describes the methodology, focusing on the multi-sensor network modelling; the second one provides a practical application to a distributed LVM system, which adopts two types of photogrammetric cameras; the third part checks the plausibility of the results of the previous application, on the basis of preliminary experiments, carried out at Politecnico di Torino—DIGEP. Section 4 summarizes the original contributions of this research, focussing on its implications, limitations and possible future developments.

2. The triangulation problem

Fig. 1 depicts a distributed LVM system based on triangulation, consisting of a number of network devices positioned around the measurement volume. *OXYZ* is a global Cartesian coordinate system. Each ith device (D_i) has its own spatial position and

[1] The adjective "accurate" is used in a broad sense, denoting the ability of a network device to perform angular measurements with relatively low uncertainty; it is not necessarily related to the specific definition from the International Vocabulary of Metrology (VIM) [18].

[2] The adjective "multi-sensor" indicates that networks include devices, which – despite they all perform angular measurements – may differ in terms of technology, accuracy, range of measurement and cost.

Please cite this article in press as: Maisano D, Mastrogiacomo L. A new methodology to design multi-sensor networks for distributed large-volume metrology systems based on triangulation. Precis Eng (2015), http://dx.doi.org/10.1016/j.precisioneng.2015.07.001

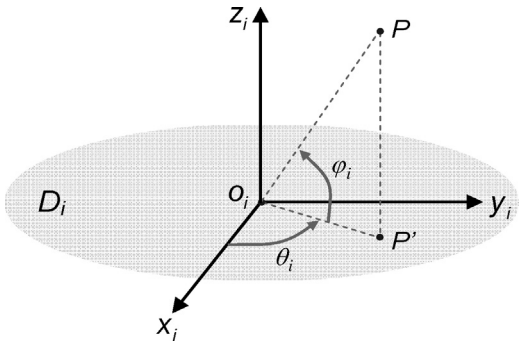

Fig. 2. For a generic network device (D_i), two angles – i.e., θ_i (azimuth) and φ_i (elevation) – are subtended by a line joining the point P (to be localized) and the origin o_i of the local coordinate system $o_i x_i y_i z_i$.

orientation, and a local coordinate system, $o_i x_i y_i z_i$, roto-translated with respect to *OXYZ*.

A general transformation between a local and the global coordinate system is:

$$\boldsymbol{X} = \boldsymbol{R_i}\boldsymbol{x_i} + \boldsymbol{X}_{0_i} \Rightarrow \begin{bmatrix} X \\ Y \\ Z \end{bmatrix} = \begin{bmatrix} r_{11_i} & r_{12_i} & r_{13_i} \\ r_{21_i} & r_{22_i} & r_{23_i} \\ r_{31_i} & r_{32_i} & r_{33_i} \end{bmatrix} \begin{bmatrix} x_i \\ y_i \\ z_i \end{bmatrix} + \begin{bmatrix} X_{0_i} \\ Y_{0_i} \\ Z_{0_i} \end{bmatrix}. \quad (1)$$

$\boldsymbol{R_i}$ is a rotation matrix, which elements are functions of three rotation parameters:

$$\boldsymbol{R}_i = \begin{bmatrix} \cos\phi_i \cos\kappa_i & -\cos\phi_i \sin\kappa_i & \sin\phi_i \\ \cos\omega_i \sin\kappa_i + \sin\omega_i \sin\phi_i \cos\kappa_i & \cos\omega_i \cos\kappa_i - \sin\omega_i \sin\phi_i \sin\kappa_i & -\sin\omega_i \cos\phi_i \\ \sin\omega_i \sin\kappa_i - \cos\omega_i \sin\phi_i \cos\kappa_i & \sin\omega_i \cos\kappa_i + \cos\omega_i \sin\phi_i \sin\kappa_i & \cos\omega_i \cos\phi_i \end{bmatrix}, \quad (2)$$

where ω_i represents a counterclockwise rotation around the x_i axis; ϕ_i represents a counterclockwise rotation around the new y_i axis, which was rotated by ω_i; κ_i represents a counterclockwise rotation around the new z_i axis, which was rotated by ω_i and then ϕ_i; for details, see [8].

$\boldsymbol{X}_{0_i} = \left[X_{0_i}, Y_{0_i}, Z_{0_i}\right]^T$ are the coordinates of the origin of $o_i x_i y_i z_i$, in the global coordinate system *OXYZ*.

The (six) location/orientation parameters related to each *i*th network device (i.e., X_{0_i}, Y_{0_i}, Z_{0_i}, ω_i, ϕ_i,κ_i) are treated as known parameters, since they are measured in an initial calibration process. The calibration process, which may vary depending on the specific technology of the measuring system, generally includes multiple measurements of calibrated artefacts, within the measurement volume [9].

The point to be localized is $P = [X, Y, Z]^T$, e.g., the position of the target in Fig. 1. From the local perspective of each *i*th device, two angles – i.e., θ_i (azimuth) and φ_i (elevation) – are subtended by the line passing through P and a local *observation point*, which we assume as coincident with the origin $o_i = [0, 0, 0]^T$ of the local coordinate system (see Fig. 2). Precisely, φ_i describes the inclination of segment o_iP with respect to the plane $x_i y_i$ (with a positive sign when $z_i > 0$), while θ_i describes the counterclockwise rotation of the projection (o_iP') of o_iP on the $x_i y_i$ plane, with respect to the x_i axis. For each *i*th local coordinate system, the following relationships hold:

$$\theta_i = \tan^{-1}\frac{y_i}{x_i} \quad \begin{cases} \text{if } x_i \geq 0 \text{ then } -\dfrac{\pi}{2} \leq \theta_i \leq \dfrac{\pi}{2} \\ \text{if } x_i < 0 \text{ then } \dfrac{\pi}{2} < \theta_i < \dfrac{3\pi}{2} \end{cases}. \quad (3)$$

$$\varphi_i = \sin^{-1}\frac{z_i}{o_iP} \quad \left\{ -\frac{\pi}{2} \leq \varphi_i \leq \frac{\pi}{2} \right.$$

Given that:

$$\tan\theta_i = \frac{\sin\theta_i}{\cos\theta_i} \quad (4)$$

and

$$o_iP = \frac{o_iP'}{\cos\varphi_i} = \frac{x_i/\cos\theta_i}{\cos\varphi_i} = \frac{x_i}{\cos\theta_i \cdot \cos\varphi_i}, \quad (5)$$

Eq. (3) can be reformulated as:

$$\begin{aligned} x_i \cdot \sin\theta_i - y_i \cdot \cos\theta_i = 0 \\ x_i \cdot \sin\varphi_i - z_i \cdot \cos\theta_i \cdot \cos\varphi_i = 0. \end{aligned} \quad (6)$$

In matrix form, Eq. (6) becomes:

$$\boldsymbol{M_i x_i} = \begin{bmatrix} \sin\theta_i & -\cos\theta_i & 0 \\ \sin\varphi_i & 0 & -\cos\theta_i \cdot \cos\varphi_i \end{bmatrix} \cdot \begin{bmatrix} x_i \\ y_i \\ z_i \end{bmatrix} = 0 \quad (7)$$

The system of two equations in Eq. (7) can be expressed as a function of the global coordinates of point P. Reversing Eq. (1), for switching from the local to the global coordinates, and considering that $\boldsymbol{R_i}$ is *orthonormal* – therefore $\boldsymbol{R_i}^{-1} = \boldsymbol{R_i}^T$ [10] – we obtain:

$$\boldsymbol{x_i} = \boldsymbol{R_i}^{-1}\left(\boldsymbol{X} - \boldsymbol{X}_{0_i}\right) = \boldsymbol{R_i}^T\left(\boldsymbol{X} - \boldsymbol{X}_{0_i}\right). \quad (8)$$

Combining Eq. (7) with Eq. (8), we obtain:

$$\boldsymbol{M_i R_i}^T\left(\boldsymbol{X} - \boldsymbol{X}_{0_i}\right) = 0, \quad (9)$$

from which:

$$\boldsymbol{M_i R_i}^T\boldsymbol{X} - \boldsymbol{M_i R_i}^T\boldsymbol{X}_{0_i} = 0. \quad (10)$$

We note that the equations of this system are linear with respect to the three (unknown) coordinates of P. Eq. (10) can be expressed in compact form, as:

$$\boldsymbol{A_i X} - \boldsymbol{B}_i = 0, \quad (11)$$

being $\boldsymbol{A}_i = \boldsymbol{M_i R_i}^T$ and $\boldsymbol{B}_i = \boldsymbol{M_i R_i}^T\boldsymbol{X}_{0_i}$.

Extending Eq. (11) to the N network devices that "see" P (i.e., those involved in the measurement process), we define a system of $2 \times N$ equations, which can be expressed in matrix form, as:

$$\boldsymbol{AX} - \boldsymbol{B} = \begin{bmatrix} \boldsymbol{A}_1 \\ \boldsymbol{A}_2 \\ \vdots \\ \boldsymbol{A}_N \end{bmatrix} \cdot \begin{bmatrix} X \\ Y \\ Z \end{bmatrix} - \begin{bmatrix} \boldsymbol{B}_1 \\ \boldsymbol{B}_2 \\ \vdots \\ \boldsymbol{B}_N \end{bmatrix} = 0. \quad (12)$$

In practice, this system is solved to determine the unknown coordinates of P, knowing several parameters relating to each *i*th network device: angles θ_i and φ_i, subtended by P, and relevant location/orientation, defined by X_{0_i}, Y_{0_i}, Z_{0_i}, ω_i, ϕ_i, andκ_i. Since the "true" values of the above parameters are never known exactly, they can be replaced with appropriate estimates: $\hat{\theta}_i$ and $\hat{\varphi}_i$, resulting from angular measurements, and $\hat{X}_{0_i}$, $\hat{Y}_{0_i}$, $\hat{Z}_{0_i}$, $\hat{\omega}_i$, $\hat{\phi}_i$, $\hat{\kappa}_i$, resulting from an initial calibration process. For this reason, from this point forward, we replace the "true" parameters with their estimates.

Please cite this article in press as: Maisano D, Mastrogiacomo L. A new methodology to design multi-sensor networks for distributed large-volume metrology systems based on triangulation. Precis Eng (2015), http://dx.doi.org/10.1016/j.precisioneng.2015.07.001

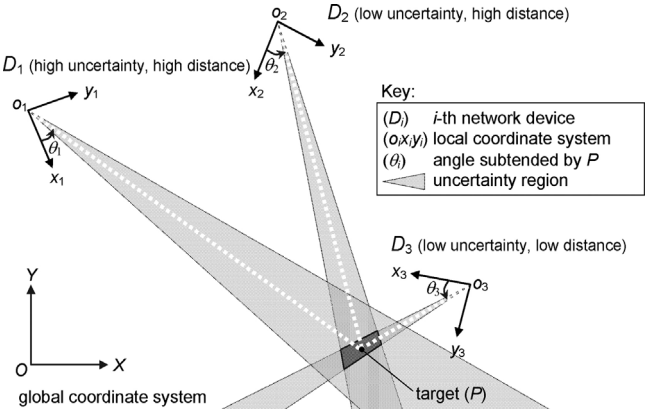

Fig. 3. 2D scheme displaying the different contributions to the uncertainty in the localization of *P*, produced by individual network devices. For each *i*th network device, the uncertainty region is triangular.

The system in Eq. (12) can be solved when *P* is "seen" by at least two devices (2 angles × 2devices = 4 total equations). Since this system is overdefined (more equations than unknown parameters), there are several possible solution approaches, ranging from those based on the iterative minimization of a suitable error function [8], to those based on the Least Squares method [11].

It is worth remarking that the equations of the system in Eq. (11) may differently contribute to the uncertainty in the localization of *P*. Specifically, two of the main factors affecting this uncertainty are:

1. *Uncertainty in angular measurements* ($\hat{\theta}_i$ and $\hat{\varphi}_i$), which generally depends on the metrological characteristics of network devices;
2. *Relative position* between the point to be localized (*P*) and each *i*th network device; in fact, assuming that the uncertainty in angular measurements is fixed, the uncertainty in the localization of *P* tends to increase proportionally to the *distance* between *P* and network devices.

The scheme in Fig. 3 makes it possible to visualize the two aforementioned factors. For simplicity, it represents a two-dimensional case, in which the localization of *P* is performed using angular measurements by three network devices, with different distance from *P* and different angular-measurement uncertainty. Assuming that each *i*th network device measures the angle (θ_i) subtended by *P* with some uncertainty, we define a triangular uncertainty region, with vertex in the origin (o_i) of the local coordinate system, bisector parallel to $\boldsymbol{o_iP}$, and vertex-angle proportional to the relevant uncertainty. Obviously, the uncertainty region tends to increase with increasing the distance between the *i*th network device and *P*.

Devices that mostly contribute to uncertainty in the localization of *P* – which can be roughly visualized by overlapping the uncertainty regions related to the three devices – are the least accurate and/or the most distant from *P*.

Returning to the system in Eq. (11), it can be said that the $2 \times N$ equations contribute to the uncertainty in the localization of *P heteroskedastically* with respect to the previous two factors. For this reason, it would be appropriate to solve this system, giving greater weight to the contributions from the network devices that produce less uncertainty and *vice versa*.

To this purpose, the most elegant and practical approach is probably that of the Generalized Least Squares (GLS) method [12], in which a weight matrix, which takes into account the uncertainty produced by the equations of the system, is defined. One of the most practical ways to define this matrix is the application of the Multivariate Law of Propagation of Uncertainty to the system in Eq. (11), referring to the parameters affected by uncertainty [13]. Assuming that such parameters are the angles measured by each *i*th device, we collect them in a vector $\boldsymbol{\xi}$:

$$\xi = \left[\hat{\theta}_1, \hat{\varphi}_1, \hat{\theta}_2, \hat{\varphi}_2, \ldots, \hat{\theta}_N, \hat{\varphi}_N\right]^T. \tag{13}$$

For simplicity, we have not taken into account the uncertainty related to the estimates of the location/orientation parameters of network devices, namely the so-called *external parameters*, contained in $\boldsymbol{X}_{0_i}$ and $\boldsymbol{R_i}$ (see Section 2), which result from calibration process [5].

Propagating the uncertainty of the equations in Eq. (11), with respect to $\boldsymbol{\xi}$, we define the weight matrix as:

$$\boldsymbol{W} = \left(\boldsymbol{J} \cdot cov\left(\xi\right) \cdot \boldsymbol{J}\right)^{-1}. \tag{14}$$

We describe in detail the elements in the second member of Eq. (14). $\boldsymbol{J}$ is the Jacobian (block-diagonal) matrix of the partial derivatives of the components of the equations in the first member of Eq. (11), with respect to the elements of $\boldsymbol{\xi}$:

$$\boldsymbol{J} = \begin{bmatrix} \boldsymbol{J}_1 & 0 & \cdots & 0 \\ 0 & \boldsymbol{J}_2 & \cdots & 0 \\ \vdots & \vdots & \ddots & \vdots \\ 0 & 0 & \cdots & \boldsymbol{J}_N \end{bmatrix}, \tag{15}$$

where the single *i*th block is defined as;

$$\boldsymbol{J_i} = \begin{bmatrix} x_i \cdot \cos\hat{\theta}_i + y_i \cdot \sin\hat{\theta}_i & 0 \\ z_i \cdot \sin\hat{\theta}_i \cdot \cos\hat{\varphi}_i & x_i \cos\hat{\varphi}_i + z_i \cdot \cos\hat{\theta}_i \cdot \sin\hat{\varphi}_i \end{bmatrix}, \tag{16}$$

and $\boldsymbol{0}$ is a 2×2 matrix of zeros.

We note that block $\boldsymbol{J_i}$ depends on the coordinates of *P*, in the local coordinate system of the *i*th network device; they can be expressed as a function of the global coordinates, by applying the transformation in Eq. (8). To define the elements in $\boldsymbol{J_i}$, *P* has therefore to be localized, at least roughly. One option is to use the Ordinary Least Squares (OLS) method [14] to solve the system in Eq. (11), as:

$$\hat{\hat{X}} = \left(\boldsymbol{A}^T\boldsymbol{A}\right)^{-1} \cdot \boldsymbol{A}^T \cdot \boldsymbol{B}, \tag{17}$$

where the "double-hat" symbol "$\hat{\hat{\ }}$" indicates that this solution is a relatively rough estimate of the final position estimate (i.e., $\hat{\boldsymbol{X}}$), which will be presented later on.

Returning to the description of Eq. (13), $\boldsymbol{\mathrm{cov}(\xi)}$ is the covariance matrix of $\boldsymbol{\xi}$, defined as

$$\boldsymbol{\mathrm{cov}}\left(\xi\right) = \begin{bmatrix} \begin{pmatrix} \sigma^2_{\hat{\theta}_1} & 0 \\ 0 & \sigma^2_{\hat{\varphi}_1} \end{pmatrix} & 0 & \cdots & 0 \\ 0 & \begin{pmatrix} \sigma^2_{\hat{\theta}_2} & 0 \\ 0 & \sigma^2_{\hat{\varphi}_2} \end{pmatrix} & \cdots & 0 \\ \vdots & \vdots & \ddots & \vdots \\ 0 & 0 & \cdots & \begin{pmatrix} \sigma^2_{\hat{\theta}_N} & 0 \\ 0 & \sigma^2_{\hat{\varphi}_N} \end{pmatrix} \end{bmatrix}, \tag{18}$$

where $\boldsymbol{0}$ is a 2×2 matrix of zeros. The diagonal elements of $\boldsymbol{\mathrm{cov}(\xi)}$ are the variances related to the angles measured by each *i*th device; in Section 3, we illustrate some practical ways to estimate these parameters. The off-diagonal entries of each *i*th block are zeros, assuming no correlation between the $\hat{\theta}_i$ and $\hat{\varphi}_i$ measurements by a generic *i*th device; the off-block-diagonal entries are zeros, assuming that network devices work independently from each other and there is no correlation between the θ_i and φ_i related to different network devices.

Please cite this article in press as: Maisano D, Mastrogiacomo L. A new methodology to design multi-sensor networks for distributed large-volume metrology systems based on triangulation. Precis Eng (2015), http://dx.doi.org/10.1016/j.precisioneng.2015.07.001

By applying the GLS method to the system in Eq. (11), we obtain the final position estimate of point P as:

$$\hat{\boldsymbol{X}} = \left(\boldsymbol{A}^T \cdot \boldsymbol{W} \cdot \boldsymbol{A}\right)^{-1} \cdot \boldsymbol{A}^T \cdot \boldsymbol{W} \cdot \boldsymbol{B}. \quad (19)$$

Summarizing, the localization of P is based on three steps: (i) rough localization of P, using the OLS method (see Eq. (16)), (ii) construction of the weight matrix $\boldsymbol{W}$ (see Eq. (13)), and (iii) final localization of P, using the GLS method (see Eq. (18)). For further details on the GLS method, see [12].

3. Proposed methodology

This section is organized into three subsections: Section 3.1 provides a general description of the proposed methodology, Section 3.2 presents a practical application example, while Section 3.3 presents an experimental check of the plausibility of the results presented in Section 3.2.

3.1. General description

As mentioned in Section 1, we consider a generic distributed LVM system, which includes two different types of network devices: (i) some accurate but expensive, hereafter classified as *type-A* devices and (ii) other less accurate but cheaper, hereafter classified as *type-B* devices.

The proposed methodology is based on three steps, which are described individually in Sections 3.1.1 to 3.1.3:

- network layout definition;
- definition of the features of network devices;
- definition and implementation of the simulations.

Section 3.1.4 sums up the basic steps of the methodology, in the form of pseudo-code concerning an ad hoc routine that was implemented in Matlab®.

3.1.1. Network layout definition

The following list contains some simplifying assumptions about the network layout relating to the distributed LVM system of interest; these assumptions reflect realistic conditions in typical working environments, such as aerospace and rail industry workshops.

We remark that LVM distributed systems are *scalable*, since network can be extended or reduced, depending on the required measurement volume [5]. For this reason, the layout definition presented in the remainder of this section is also scalable.

- The network covers an appropriate *measuring volume*, characterized by a surface (S) of the order of magnitude of several tens of squared meters and height from the floor level of about 3 m.
- Network devices are positioned according to a regular grid with square meshes (with side s), in the centre of which network devices are positioned (see the example in Fig. 4). The network *density*, i.e., the number of network devices per surface unit, is defined as:

$$\delta = \frac{1}{s^2}. \quad (20)$$

For example, in the network exemplified in Fig. 4, $\delta = 1/(2\,\text{m})^2 = 0.25$ devices/m^2.
- Network devices are positioned with appropriate orientation and height with respect to the floor level, so as to cover the largest possible measurement volume. These features may depend on the network devices in use; for example, photogrammetric cameras are generally positioned at a height of approximately 4 to 5 m and oriented downwards, while optical theodolites and R-LATs are generally positioned at a height of about 1.5 m, with vertical z_i axis.
- For simplicity, we exclude the presence of obstacles between network devices and points to be localized.
- The *mix* between type-A and B network devices is defined using the following (complementary) parameters:

$$p_A = \frac{\text{TypeA devices}}{\text{Total network devices}},$$
$$p_B = 1 - p_A = \frac{\text{TypeB devices}}{\text{Total network devices}}. \quad (21)$$

E.g., the network exemplified in Fig. 4 consists of 50 network devices, including 10 type-A devices and 40 type-B devices, therefore $p_A = 20\%$ and $p_B = 80\%$. The distribution of these devices is random, provided that they are positioned in the predetermined positions, i.e., at the centre of the meshes of the grid.
- The parameters δ and p_A (defined in Eqs. (20) and (21), respectively) are changed at multiple levels, defining a number (C) of *configurations*. For example, having defined 4 levels for δ and 5 for p_A, there will be total $4 \times 5 = 20$ configurations.

3.1.2. Definition of the features of network devices

The proposed procedure requires the definition of several technical/metrological features concerning network devices, as follows:

- Definition of the *angular-measurement uncertainty* of each ith network device, in the form of standard deviations σ_{θ_i} and σ_{φ_i}. These parameters can be obtained in several ways: (i) from manuals or technical documents relating to the network devices in use, (ii) estimated through ad hoc experimental tests, or (iii) estimated using data from previous calibration processes. We remark that the σ_{θ_i} and σ_{φ_i} values should reflect the network devices' uncertainty in realistic working conditions, e.g., in the presence of vibrations, light/temperature variations and other typical disturbance factors. Obviously, type-A network devices will be characterized by lower uncertainties, with respect to type-B ones.
- Definition of the *uncertainty in the location/orientation* of network devices, in the form of variances $\sigma^2_{X_{0_i}}, \sigma^2_{Y_{0_i}}, \sigma^2_{Z_{0_i}}, \sigma^2_{\omega_i}, \sigma^2_{\phi_i}, \sigma^2_{\kappa_i}$. These uncertainties may depend on several features characterizing the calibration process (e.g., amount of measurements, size of the calibrated artefacts in use, etc.) [15].
- Definition of the *range of measurement* of each network device, usually expressed in terms of (i) maximum distance range (d_{MAX}) between the network device and the point to be located and (ii) minimum and maximum angular range, relating to the elevation angle (i.e., φ_{MIN},φ_{MAX}). For example, a medium-quality photogrammetric camera has $d_{MAX} \approx 6$ to 8 m, $\varphi_{MIN} \approx 45^\circ$ and $\varphi_{MAX} \approx 90^\circ$; on the other hand, an R-LAT has $d_{MAX} \approx 20$ m, $\varphi_{MIN} \approx -40^\circ$ and $\varphi_{MAX} \approx 40^\circ$ [5].
- Definition of the purchase cost of network devices; of course, the purchase cost of type-A cameras (i.e., C_A) is likely to be higher than that of type-B ones (i.e., C_B). Combining these data with those relating to surface density (δ) and mix between type-A and B network devices (p_A), we define the network's *cost per surface unit*, as:

$$c = [p_A \cdot C_A + p_B \cdot C_B] \cdot \delta = [p_A \cdot C_A + (1 - p_A) \cdot C_B] \cdot \delta. \quad (22)$$

Obviously, the total cost of a network, which covers a surface S, will be given by the product $S \times c$.

3.1.3. Definition and implementation of the simulations

Based on the assumptions about network layout and the characteristics of network devices (defined in Sections 3.1.1 and 3.1.2,

Please cite this article in press as: Maisano D, Mastrogiacomo L. A new methodology to design multi-sensor networks for distributed large-volume metrology systems based on triangulation. Precis Eng (2015), http://dx.doi.org/10.1016/j.precisioneng.2015.07.001

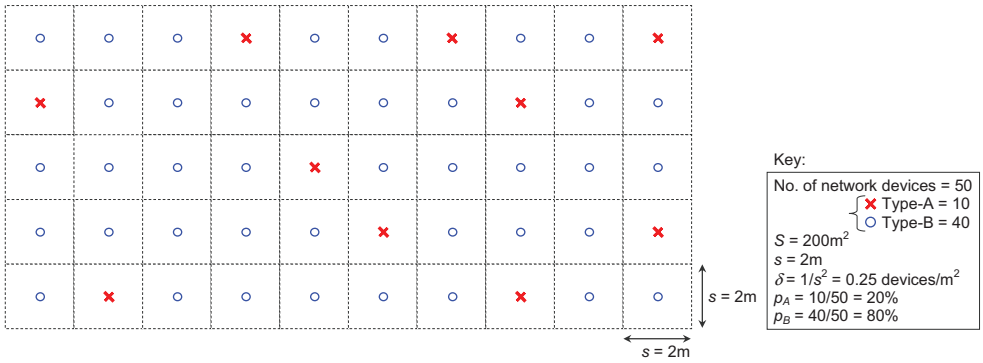

Fig. 4. Example of network layout (plan view).

respectively), we now analyse the performance of different network configurations, obtained by varying the parameters δ and p_A. To this purpose, we define a large number of simulated experiments, as follows.

For each configuration, we define a number (R) of *repositionings*—i.e., random assignments of (type-A and B) network devices to the predetermined positions of the grid. Fig. 4 shows one of the possible repositionings for a configuration with $\delta = 0.25$ devices/m^2 and $p_A = 20\%$.

The decision to perform multiple repositionings is aimed at analyzing the "average" metrological performance of not-necessarily-identical networks, characterized by the same parameters δ and p_A. For each repositioning, the "true" location/orientation of network devices is deliberately distorted, to take account of the uncertainties resulting from calibration process; in formal terms, we determine:

$$\begin{aligned}
\hat{X}_{0_i} &= X_{0_i} + \varepsilon_{X_{0_i}} \quad \text{being} \quad \varepsilon_{X_{0_i}} \sim N\left(0, \sigma^2_{X_{0_i}}\right) \\
\hat{Y}_{0_i} &= Y_{0_i} + \varepsilon_{Y_{0_i}} \quad \text{being} \quad \varepsilon_{Y_{0_i}} \sim N\left(0, \sigma^2_{Y_{0_i}}\right) \\
\hat{Z}_{0_i} &= Z_{0_i} + \varepsilon_{Z_{0_i}} \quad \text{being} \quad \varepsilon_{Z_{0_i}} \sim N\left(0, \sigma^2_{Z_{0_i}}\right) \\
\hat{\omega}_i &= \omega_i + \varepsilon_{\omega_i} \quad \text{being} \quad \varepsilon_{\omega_i} \sim N\left(0, \sigma^2_{\omega_i}\right) \\
\hat{\phi}_i &= \phi_i + \varepsilon_{\phi_i} \quad \text{being} \quad \varepsilon_{\phi_i} \sim N\left(0, \sigma^2_{\phi_i}\right) \\
\hat{\kappa}_i &= \kappa_i + \varepsilon_{\kappa_i} \quad \text{being} \quad \varepsilon_{\kappa_i} \sim N\left(0, \sigma^2_{\kappa_i}\right)
\end{aligned} \tag{23}$$

i.e., the parameters related to the "true" location/orientation of each ith network device are distorted by adding zero-mean normally distributed errors, with known variances. This hypothesis is reasonable in the absence of systematic error causes. Given that the errors resulting from calibration are generally related to the technical/metrological characteristics of network devices [15], it is reasonable to assume that devices of the same type (A or B) are characterized by the same calibration errors. Also, in the absence of spatial/directional effects, it is reasonable to assume that these errors are *isotropic*, i.e., they are uniformly spread over the three spatial directions. In formal terms:

$$\begin{aligned}
\sigma^2_{X_{0_i}} = \sigma^2_{Y_{0_i}} = \sigma^2_{Z_{0_i}} = & \begin{cases} \sigma^2_{X_{0_A}} & \forall\, i\text{th device of typeA} \\ \sigma^2_{X_{0_B}} & \forall\, i\text{th device of typeB} \end{cases} \\
\sigma^2_{\omega_i} = \sigma^2_{\phi_i} = \sigma^2_{\kappa_i} = & \begin{cases} \sigma^2_{\omega_A} & \forall\, i\text{th device of typeA} \\ \sigma^2_{\omega_B} & \forall\, i\text{th device of typeB} \end{cases}
\end{aligned} . \tag{24}$$

Subsequently, for each of the R repositionings, we randomly generate a number (M) of points, distributed uniformly within the measurement volume. Since the true position of each point is known a priori, it is possible to (i) identify the subset of network devices, which include the point in their range of measurement, and (ii) calculate the "true" angles subtended by the point with respect to these network devices (using the formulae in Eq. (3)). To take the angular-measurement uncertainty into account, the true angles (i.e., θ_i and φ_i) are deliberately distorted:

$$\begin{aligned}
\hat{\theta}_i &= \theta_i + \varepsilon_{\theta_i} \quad \text{being} \quad \varepsilon_{\theta_i} \sim N\left(0, \sigma^2_{\theta_i}\right) \\
\hat{\varphi}_i &= \varphi_i + \varepsilon_{\varphi_i} \quad \text{being} \quad \varepsilon_{\varphi_i} \sim N\left(0, \sigma^2_{\varphi_i}\right)
\end{aligned} , \tag{25}$$

where ε_{θ_i} and ε_{φ_i} are zero-mean normally distributed random errors, with variances $\sigma^2_{\theta_i}$ and $\sigma^2_{\varphi_i}$, respectively. In the absence of systematic error causes and spatial/directional effects, it is reasonable to assume that (i) for each ith network device, the two variances are coincident, and (ii) devices of the same type are characterized by the same variances; in formal terms:

$$\sigma^2_{\theta_i} = \sigma^2_{\varphi_i} = \begin{cases} \sigma^2_{\theta_A} & \forall\, i\text{th device of type A} \\ \sigma^2_{\theta_B} & \forall\, i\text{th device of type B} \end{cases} . \tag{26}$$

Based upon this assumption, the matrix $\mathbf{cov}(\boldsymbol{\xi})$ (in Eq. (18)) is greatly simplified, as it includes only two parameters (i.e., $\sigma^2_{\theta_A}$ and $\sigma^2_{\theta_B}$), repeated depending on the number of type-A and type-B cameras involved in the measurement.

For each jth point related to a certain rth repositioning of network devices, we define N as the number of network devices that can "see" the point, since they include it in their range of measurement. If $N \geq 2$, the localization can be simulated and the position error can be estimated as:

$$\begin{aligned}
\varepsilon_{P_{j,r}} &= \left\| \hat{\boldsymbol{X}}_{j,r} - \boldsymbol{X}_{j,r} \right\| \\
&= \sqrt{\left(\hat{X}_{j,r} - X_{j,r}\right)^2 + \left(\hat{Y}_{j,r} - Y_{j,r}\right)^2 + \left(\hat{Z}_{j,r} - Z_{j,r}\right)^2},
\end{aligned} \tag{27}$$

being $\boldsymbol{X}_{j,r} = \left[X_{j,r}, Y_{j,r}, Z_{j,r}\right]^T$ the true position of the point to be located, which is known a priori, and $\hat{\boldsymbol{X}}_{j,r} = \left[\hat{X}_{j,r}, \hat{Y}_{j,r}, \hat{Z}_{j,r}\right]^T$ the localization obtained by applying the model illustrated in Section 2.

If $N < 2$, the jth point cannot be localized. For each repositioning, we define L_r as the set including the subscripts (j) of the points that can be localized; the number of elements in L_r is:

$$m_r = |L_r| \leq M, \tag{28}$$

where the symbol "$|L_r|$" denotes the cardinality of set L_r.

Repeating the exercise for the totality of the (M) points in each rth repositioning, we can determine the distribution of the position

Please cite this article in press as: Maisano D, Mastrogiacomo L. A new methodology to design multi-sensor networks for distributed large-volume metrology systems based on triangulation. Precis Eng (2015), http://dx.doi.org/10.1016/j.precisioneng.2015.07.001

error relating to the configuration examined, as the union of all the $\varepsilon_{P_{j,r}}$ values available. The total number of realizations of $\varepsilon_{P_{j,r}}$ is $\sum_{r=1}^{R} m_r \leq R \cdot M$. We now define an indicator of the (average) *coverage level* related to a certain network configuration, as the ratio between the number of localized points and the overall number of simulated points:

$$Cvg = \frac{\sum_{r=1}^{R} m_r}{R \cdot M}. \tag{29}$$

Obviously, $Cvg \in [0, 1]$; this indicator will tend to decrease for networks characterized by low density (δ) and/or network devices with relatively small range of measurement.

Next, we calculate the following statistics, concerning the $\varepsilon_{P_{j,r}}$ distribution:

$$\mu_P = \frac{1}{\sum_{r=1}^{R} m_r} \sum_{r=1}^{R} \sum_{\forall j \in L_r} \varepsilon_{P_{j,r}}$$
$$\sigma_P = \sqrt{\frac{\sum_{r=1}^{R} \sum_{\forall j \in L_r} \left(\varepsilon_{P_{j,r}} - \mu_P\right)^2}{\left(\sum_{r=1}^{R} m_r\right) - 1}}, \tag{30}$$

Due to the definition of $\varepsilon_{P_{j,r}}$, the two indicators μ_P and σ_P will always be larger than or equal to 0.

Data resulting from simulations can be also used for estimating the uncertainty relating to distance measurements. To this purpose, we consider all the possible pairs of points in each repositioning; since the number of localized points in a certain repositioning is m_r, the total number of possible pairs of points (and relevant distances) will be $C_2^{m_r} = (m_r!)/(2!\,(m_r - 2)!)$. We can define the distance error as:

$$\varepsilon_{d_{jk,r}} = \hat{d}_{jk,r} - d_{jk,r} = \left\|\hat{\boldsymbol{X}}_{j,r} - \hat{\boldsymbol{X}}_{k,r}\right\| - \left\|\boldsymbol{X}_{j,r} - \boldsymbol{X}_{k,r}\right\|, \tag{31}$$

being $\hat{\boldsymbol{X}}_{j,r}$ and $\hat{\boldsymbol{X}}_{k,r}$ the estimated positions of the jth and kth point (where j and $k \in L_r$); $\boldsymbol{X}_{j,r}$ and $\boldsymbol{X}_{k,r}$ the relevant true positions (known a priori).

Considering the totality of pairs for all the R repositionings, we can determine the distribution of the distance error, for the configuration of interest, as the union of all the $\varepsilon_{d_{jk,r}}$ values. Next, we calculate the following statistics:

$$\mu_d = \frac{1}{R \cdot C_2^{m_r}} \sum_{r=1}^{R} \sum_{\forall j \in L_r} \sum_{\forall k \in L_r : k > j} \varepsilon_{d_{jk,r}}$$
$$\sigma_d = \sqrt{\frac{\sum_{r=1}^{R} \sum_{\forall j \in L_r} \sum_{\forall k \in L_r : k > j} \left(\varepsilon_{d_{jk,r}} - \mu_d\right)^2}{\left(\sum_{r=1}^{R} C_2^{m_r}\right) - 1}}, \tag{32}$$

Due to the definition of $\varepsilon_{d_{jk,r}}$, the indicator μ_d is expected to be roughly 0, while $\sigma_d \geq 0$. Between μ_d and σ_d, σ_d is the most representative statistic for distance-measurement uncertainty. Also, using σ_d values is more practical than using μ_P or σ_P values; the reason is that typical industrial applications concern the dimensional verification of distances between pairs of points on the object of interest (e.g., point clouds depicting the object's surface) and not the absolute position of these points.

Finally, the cost per surface unit (c) relating to each configuration can be estimated using Eq. (22).

The so-far-described procedure should be extended to the totality of the network configurations. The large amount of data resulting from this analysis can be organized into appropriate tables and graphs, which are illustrated in Section 3.2.

3.1.4. Ad hoc routine

The methodology illustrated in the previous three sub-sections has been automated by an ad hoc routine developed in Matlab®; the following pseudo-code summarizes the basic steps of this routine:

Network Layout definition
1. Define the features of the measuring volume (e.g., surface, maximum height from the floor level, etc.).
2. Define the levels of δ and p_A, which characterize the (C) configurations.

Definition of the features of the network devices
3. For each of the two types (A and B) of network devices:
4. Set the uncertainty in angular measurements.
5. Define their orientation/height with respect to the floor level.
6. Set the uncertainty in location/orientation, resulting from calibration.
7. Set the typical range of measurement.
8. Set the unitary cost.
9. End For.

Definition and implementation of the simulations
10. For each of the C configurations:
11. Determine the cost per surface unit (c), using Eq. (22).
12. Define the number of repositionings (R) of the network devices.
13. For each rth of the R repositionings:
14. Randomly assign type-A and B network devices to the predetermined positions (on the grid).
15. Distort the true location/orientation of each network device, in order to take account of the uncertainties resulting from calibration (Eq. (23)).
16. Define M points, randomly distributed over the measuring volume.
17. For each of the M points:
18. Determine the portion of N devices, which can "see" the point.
19. If $N \geq 2$:
20. For each of these N devices:
21. Calculate the true θ_i and φ_i angles, using Eq. (3).
22. Distort the true angles, in order to take account of the angular-measurement uncertainty (Eq. (25)).
23. End For.
24. Localize the point, applying the mathematical model in Eq. (19).
25. Calculate the position error (Eq. (27)).
26. End if.
27. End For.
28. For each of the possible ($C_2^{m_r}$) pairs of points:
29. Determine the "true" and estimated distance, then the corresponding distance error (Eq. (32)).
31. End For.
32. End For.
33. Determine the indicator Cvg, depicting the coverage level (Eq. (29)).
34. Perform the union of the (available) position errors and determine the statistics in Eq. (30).
35. Perform the union of the (available) distance-measurement errors and determine the statistics in Eq. (32).
36. End For.
37. Generate appropriate tables and charts, representing the results obtained.
38. End.

3.2. Application example

This section presents a practical application of the methodology described in Section 3.1, to design a multi-sensor network for a low-end distributed LVM system, based on infrared (IR) photogrammetry. Before going into the description of the application, Section 3.2.1 makes a brief digression to recall some basic concepts about photogrammetric systems in general. Section 3.2.2 focuses on the definition of the network layout, the features of network devices, and the simulated experiments. Section 3.2.3 presents and comments the results of the simulations.

Please cite this article in press as: Maisano D, Mastrogiacomo L. A new methodology to design multi-sensor networks for distributed large-volume metrology systems based on triangulation. Precis Eng (2015), http://dx.doi.org/10.1016/j.precisioneng.2015.07.001

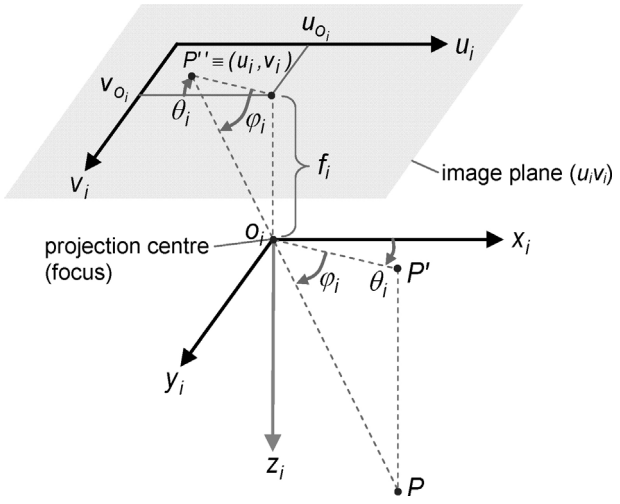

Fig. 5. For a generic ith network camera, representation of the local coordinate system, with origin (o_i) in the projection centre (or focus), and the image plane $u_i v_i$, parallel to the plane $x_i y_i$, at a distance f_i (i.e., the focal length).

3.2.1. Basic concepts on photogrammetric systems

For most of the existing systems, network devices are IR cameras associated with IR illuminators, while targets are reflective spheres, whose centres should be localized. Reflective spheres are passive targets illuminated by the illuminators. Alternatively, one can use active spherical targets that emit IR light, not making it necessary to use illuminators.

The measurement uncertainty of photogrammetric systems generally depends on the cameras in use: high pixel resolution and good quality lens help in reducing measurement uncertainty for static measurements, while high frame rate helps in reducing measurement uncertainty for dynamic measurements.

We now focus the attention on each ith network camera. The angles θ_i and φ_i are not measured directly: each ith network camera measures the coordinates of $P'' \equiv (u_i, v_i)$, i.e., the projection of target P on the camera's image plane $u_i v_i$, which is parallel to the plane $x_i y_i$ of the local coordinate system. Knowing these coordinates and the camera focal length (f_i), it is possible to estimate θ_i and φ_i (see Fig. 5):

$$\hat{\theta}_i = \tan^{-1}\frac{v_i - v_{0_i}}{u_i - u_{0_i}} \qquad \begin{cases} \text{if} \quad u_i - u_{0_i} > 0 \quad \text{then} \quad \dfrac{\pi}{2} < \theta_i < \dfrac{3\pi}{2} \\ \text{if} \quad u_i - u_{0_i} \le 0 \quad \text{then} \quad -\dfrac{\pi}{2} \le \theta_i \le \dfrac{\pi}{2} \end{cases}$$

$$\hat{\varphi}_i = \tan^{-1}\frac{f_i}{\sqrt{\left(u_i - u_{0_i}\right)^2 + \left(v_i - v_{0_i}\right)^2}} \qquad \left\{ -\frac{\pi}{2} \le \varphi_i \le \frac{\pi}{2} \right. \tag{33}$$

where u_i and v_i are the coordinates of the projection (P'') of P on the image plane; u_{0_i} and v_{0_i} are the coordinates of the projection of o_i on the image plane; f_i is the distance between the plane $u_i v_i$ and the camera projection centre (or focus), which is coincident with the origin o_i of the local coordinate system $o_i x_i y_i z_i$.

3.2.2. Definition of the simulations

We assume that the photogrammetric system of interest includes two types of network cameras:

1. *Type-A*: Hitachi, Gigabit Ethernet Infrared cameras, with 1360 × 1024 pixel resolution and 30 fps;
2. *Type-B*: PixArt/WiiMote Infrared cameras, with 126 × 96 pixel resolution and 100 fps.

It is worth noting that, while type-A cameras are professional products of good quality, type-B cameras can be classified as toy cameras.

The list below reports some assumptions about the layout of network cameras and the measurement volume.

- Network cameras are positioned on the ceiling, at 4.5 m in height from the floor, facing down and positioned at the centre of the square meshes (with side s) of the grid;
- The parameter δ (or s) is changed on 14 levels (i.e., s = 0.75, 1, 1.25, 1.5, 1.75, 2, 2.25, 2.5, 2.75, 3, 3.25, 3.5, 3.75 and 4 m), while parameter p_A on 10 levels (i.e., p_A = 0%, 2.5%, 5%, 7.5%, 10%, 12.5%, 15%, 17.5%, 20%, 22.5%), for total $C = 14 \times 10 = 140$ configurations. For each configuration, we define R = 200 random repositionings of network devices. For each rth repositioning, we generate M = 100 points (to be localized), distributed uniformly in the measurement volume. Among these M points, those that can be localized – since they are within the range of measurement of at least two network devices –are $m_r \le M$. The $C_2^{m_r}$ possible pairs of points determine as many corresponding distances. In the case of perfect coverage, i.e., when all the M points in each repositioning can be localized, the total number of points and distances available are, respectively, $R \times M = 200 \times 100 = 20{,}000$ and $R \times C_2^{100} = 200 \times 4950 = 990{,}000$ for a generic configuration. The measurement volume (which includes the randomly generated points) is a parallelepiped region with surface $S = 15 \times 15 = 225\ \text{m}^2$ and height from the floor level of 3 m. This way, we exclude "low coverage" regions, i.e., regions at relatively large height, which are poorly covered by the range of measurement of network cameras; details on the range of measurement of network devices will be given in the next paragraph.

Table 1 reports the technical/metrological features of the network devices in use. Data concerning the angular-measurement uncertainty are obtained through preliminary experimental tests. Uncertainties relating to the location/orientation of network devices can be obtained from previous calibration processes; the fact that the uncertainties related to type-A cameras are generally lower than those related to type-B cameras is a consequence of the lower angular-measurement uncertainty [16].

The range of measurement of each ith device is a cone with axis parallel to z_i axis (of the local coordinate system), vertex at the origin o_i, vertex-angle $2 \times (90^\circ - \varphi_{MIN})$, surmounting a spherical cap centred in o_i and with radius d_{MAX} (see Fig. 6). Knowing the range of measurement of network devices, we can determine, for each of the simulated points, the set of (N) cameras involved in the measurement and then determine whether the point can be localized (i.e., $N \ge 2$).

For each of the R repositionings, the true position/orientation of network cameras are deliberately distorted, as described in Eq. (23). For each of the M points, the true angles related to each device are distorted too, as described in Eq. (25). Next, when $N \ge 2$, localization is simulated and position error is calculated using Eq. (27). For each

Please cite this article in press as: Maisano D, Mastrogiacomo L. A new methodology to design multi-sensor networks for distributed large-volume metrology systems based on triangulation. Precis Eng (2015), http://dx.doi.org/10.1016/j.precisioneng.2015.07.001

Table 1
Technical/metrological features of the (type-A and B) network cameras..

	Type-A camera	Type-B camera
Model	Hitachi, Gigabit Ethernet	PixArt/WiiMote
Pixel resolution	1360 × 1024	126 × 96
Frame rate	≈30 fps	≈100 fps
Light type	Infrared	Infrared
Uncertainty in angular measurement $\left(\sigma_{\theta_i}\right)$	≈0.02°	≈0.3°
Location uncertainty $\left(\sigma_{X_{0_i}}\right)$, from calibration	≈0.08 mm	≈1.1 mm
Orientation uncertainty $\left(\sigma_{\omega_i}\right)$, from calibration	≈0.02°	≈0.1°
Range of measurement		
φ_{MIN}	≈40°	≈45°
φ_{MAX}	≈90°	≈90°
d_{MAX}	≈8 m	≈6 m
Purchase cost	≈350 €	≈40 €

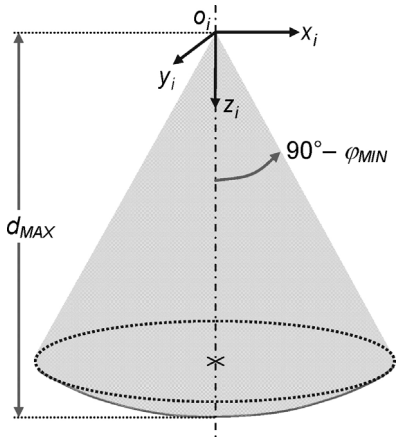

Fig. 6. Range of measurement of a generic (*i*th) photogrammetric camera.

configuration, we therefore have several thousands of realizations of the position error, forming a distribution for which we determine the statistics in Eq. (30).

Considering the totality of the pairs of points in each configuration, it is possible to estimate the relevant distance errors, using the relationship in Eq. (31). We therefore have hundreds of thousands of realizations of the distance-measurement error, forming a distribution for which we determine the statistics in Eq. (32).

Finally, for each configuration, the *Cvg* indicator and the cost per surface unit are determined by applying Eqs. (29) and (22), respectively.

3.2.3. Results

Table A.1 (in Appendix A) summarizes the results of the simulations. Each row is related to one of the 140 configurations examined. It can be noticed that the statistics relating to measurement uncertainty (e.g., μ_P, σ_P, μ_d, and σ_d) are relatively high. i.e., in the order of magnitude of a few mm. This is due to the fact that the modelled network includes two types of cameras with a very clear gap in terms of metrological performance; given that the majority of the cameras (i.e., those of type-B) are not very accurate, the resulting measurement uncertainty will be inevitably large.

Not surprisingly, the higher the parameters δ and p_A, the lower the measurement uncertainty (both in terms of σ_P and σ_d) and the higher *c*. In addition, the network configurations with relatively low network density are the ones with the poorest coverage; reversing the perspective, it can be noticed that the first 40 configurations in Table A.1 (in Appendix A) have $Cvg \geq 95\%$, due to their relatively high δ values.

Fig. 7 displays the results in a more intuitive way, through two 3D surfaces (and relevant contour lines) representing, respectively, σ_d and *c* as functions of both δ and p_A. Also, in the graphs containing the contour lines, we identify three regions with different coverage levels: respectively $Cvg < 95\%$, $95\% \leq Cvg < 99\%$, and $Cvg \geq 99\%$.

These graphs show that a good strategy to achieve a certain σ_d (and *Cvg*), without making *c* increase excessively, is selecting a sufficiently high p_A and reducing δ to the necessary extent, consistently with the requested σ_d. For example, assuming that the required $\sigma_d \leq 5$ mm and $Cvg \geq 95\%$, the network configuration that minimizes *c* is the one with $\delta = 0.44$ devices/m^2 and $p_A = 17.5\%$ (see the configuration no. 33 in Table A.1).

The same result can be obtained looking through the maps in Fig. 8, obtained by superimposing the *iso*-σ_d contour lines (i.e., σ_d = constant) with *iso*-*c* (i.e., *c* = constant). This graph also shows that, as expected, low uncertainties are often incompatible with low costs.

In the previous graphs, σ_d (not σ_P) is used as indicator of measurement uncertainty. The fact remains that σ_d and σ_P are strongly correlated by an approximately linear relationship (e.g., $R^2 \approx 95\%$ considering the data in Table A.1).

3.3. Preliminary experiments

To check the plausibility of the results presented in Section 3.2, we perform some experiments on a low-end IR photogrammetric system. This system has been developed at the industrial and quality engineering laboratory of DIGEP—Politecnico di Torino and includes the same two types of network cameras described in Table 1.

It is assumed that (i) floor area of the measurement volume is $S \approx 6 \times 5 = 30$ m^2, (ii) required uncertainty on distance measurement is $\sigma_d \approx 2.5$ mm and (iii) total budget is 3000€. The maximum cost per surface unit is therefore $c = 3000€/30\,\text{m}^2 \approx 100€/\text{m}^2$.

Table A.1 shows that the cheapest configuration, compatible with the required σ_d is that with $\delta = 1$ device/m^2 (or $s = 1$ m) and $p_A = 15\%$ (see configuration no. 14 in Table A.1); for this configuration $c = 86.5€/\text{m}^2$ and $Cvg \approx 100\%$. Interestingly, the budget is also compatible with a configuration with a σ_d even lower than the required one: in fact, configuration no. 13 in Table A.1 – with $\delta = 1$ device/m^2 (or $s = 1$ m) and $p_A = 17.5\%$ – is associated with $\sigma_d \approx 2.21$ mm and $c \approx 94.3€/\text{m}^2$.

Adopting the latter configuration, we set a network with $S \times \delta = 30$ total cameras, among which $p_A \times S \times \delta \approx [5.25] = 5$ of type-A and $p_B \times S \times \delta \approx [24.75] = 25$ of type-B. We remark that, after rounding the number of type-A and B cameras to the nearest integer, there is a slight reduction in *c*, from $94.3€/\text{m}^2$ to $91.7€/\text{m}^2$ (calculated using Eq. (22)). The resulting total cost of the network is therefore $S \times \delta \approx = 2750€$. Also, there is a slight reduction in p_A, from 17.5% to 5/30 ≈ 16.7%.

Cameras are arranged at the centre of square meshes with side $s \approx 1$ m of a regular grid, at a 4.5 m height from the floor (in line with the assumption of the model used in Section 3.2). Type-A and B cameras are distributed relatively uniformly over the predetermined positions[3]; Fig. 9 contains a scheme of the experimental network layout. The location/orientation of network devices are determined through a calibration process, based on multiple measurements of calibrated artefacts, within the measurement volume [16].

Next, we perform some dimensional measurements using three calibrated bars of different lengths: about 1 m, 1.5 m and 2 m (see

[3] In general, a uniform distribution of type-A cameras helps in limiting areas with relatively high uncertainty, since they are exclusively covered by type-B cameras.

Please cite this article in press as: Maisano D, Mastrogiacomo L. A new methodology to design multi-sensor networks for distributed large-volume metrology systems based on triangulation. Precis Eng (2015), http://dx.doi.org/10.1016/j.precisioneng.2015.07.001

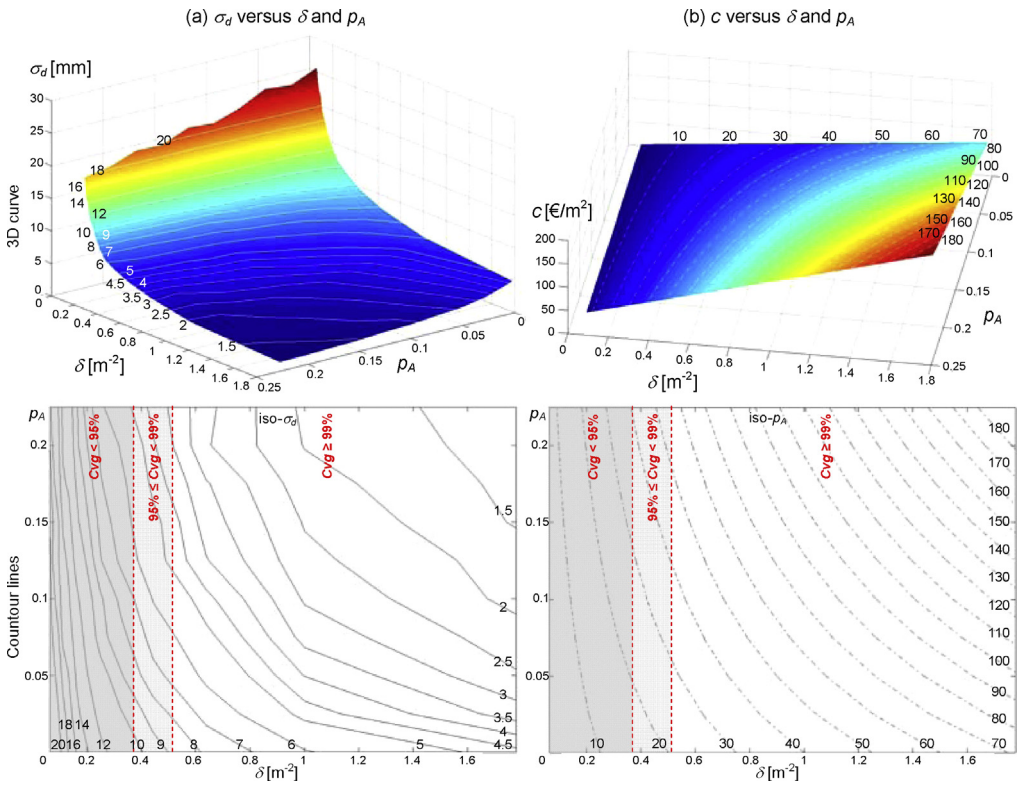

Fig. 7. 3D surfaces and corresponding contour lines related to the data in Table A.1 (in Appendix A). The figures on surfaces and contour lines, refer to the relevant σ_d and c values. Regarding contour lines, the p_A-δ plan is divided in three regions: (i) $Cvg < 95\%$, (ii) $95\% \leq Cvg < 99\%$, and (iii) $Cvg \leq 99\%$.

Fig. 10). The true values of these lengths were measured with a Coordinate Measuring Machine (CMM) with measurement uncertainty of the order of magnitude of a few tenths of μm, i.e., at least 2–3 orders of magnitude lower than the (purported) measurement uncertainty of the photogrammetric system in use [17].

For each of the three calibrated bars, we place two targets at the two ends of the bar and perform 50 measurements, in different positions within the measurement volume. Specifically, in each measurement, targets are localized and the length of the bar is calculated as Euclidean distance between the two targets. The total number of distance measurements is therefore 150.

The distance error is defined as:

$$\varepsilon_{d_{jk}} = \hat{d}_{jk} - d_{jk}, \tag{34}$$

being $\hat{d}_{jk}$ is the distance calculated using the relationship $\left\|\hat{\boldsymbol{X}}_j - \hat{\boldsymbol{X}}_k\right\|$, where $\hat{\boldsymbol{X}}_j$ and $\hat{\boldsymbol{X}}_k$ are the estimated positions of the two targets; d_{jk} is the "true" value of d_{jk} (determined using the CMM).

Aggregating the 150 distance-measurement errors, we construct the experimental distribution of the $\varepsilon_{d_{jk}}$ values and determine the statistics reported in Eq. (32). These statistics are compared with those obtained from simulations, for a similar

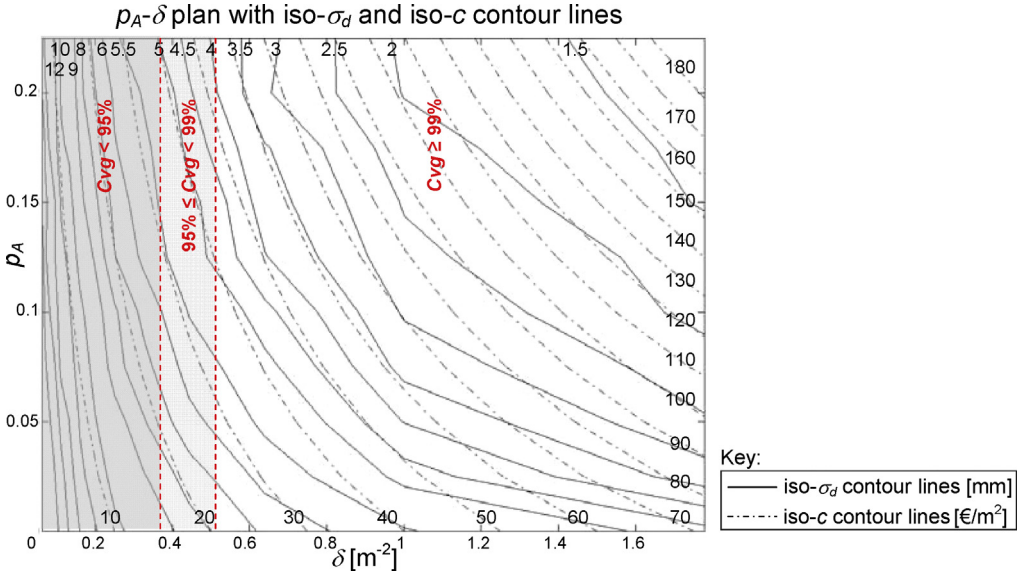

Fig. 8. Map representing the iso-σ_d (i.e., σ_d = constant) and iso-c contour lines (i.e., c = constant) relating to Fig. 7. The figures in the bottom/right side refer to iso-c contour lines, while figures in the top side refer to iso-σ_d contour lines.

Please cite this article in press as: Maisano D, Mastrogiacomo L. A new methodology to design multi-sensor networks for distributed large-volume metrology systems based on triangulation. Precis Eng (2015), http://dx.doi.org/10.1016/j.precisioneng.2015.07.001

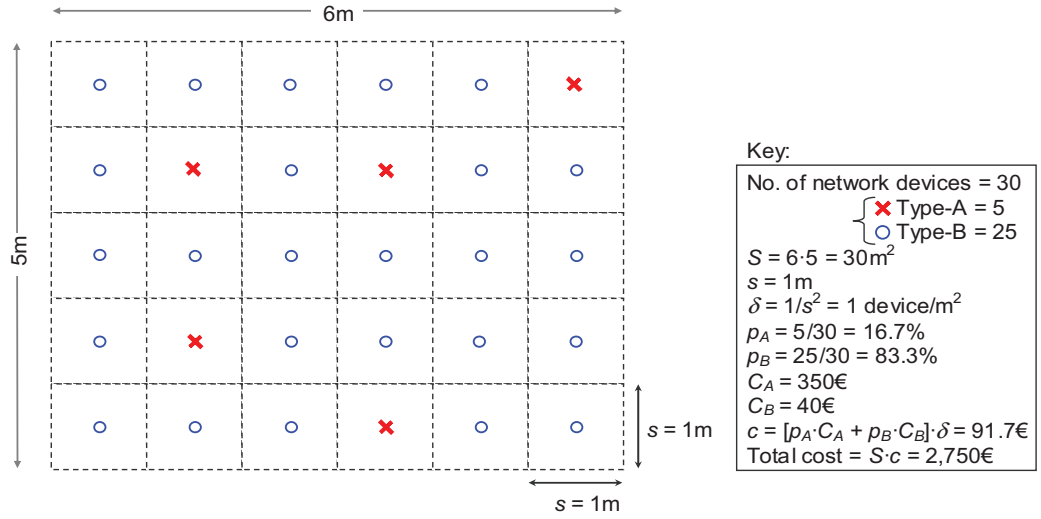

Fig. 9. Scheme of the experimental network layout (plan view).

Table 2
Comparison between the results obtained from simulated and actual experiments, for a certain network configuration.

	δ [m^{-2}]	s [m]	p_A [%]	c [€/m^2]	Cvg [%]	μ_d [mm]	σ_d [mm]
Simulations	1	1	17.5	94.3	100.0	0.03	2.21
Experiments	1	1	16.7	91.7	100.0	0.07	2.15

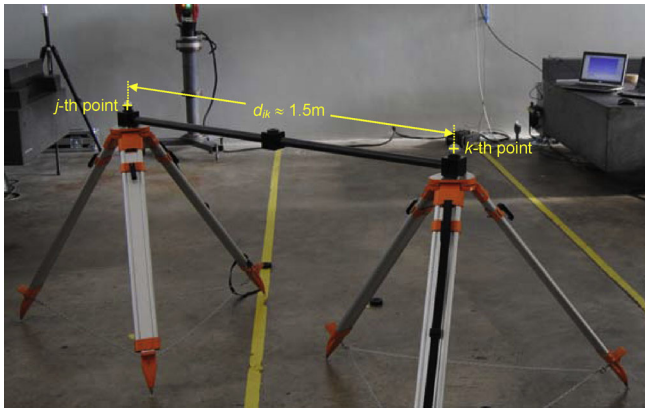

Fig. 10. Photo of one of the calibrated bars used for the experiments.

configuration (i.e., the statistics concerning configuration no. 13, in Table A.1) (Table 2).

The agreement between these data is comforting, since it indicates that the proposed methodology is feasible and provides plausible results. In particular, it can be noticed that the σ_d estimated experimentally is very close to that resulting from simulations. This result is also remarkable, in light of the fact that the p_A used in the experiments is slightly lower than that used in the simulations.

4. Concluding remarks

This paper proposed a methodology to support the design of networks for distributed LVM systems based on triangulation. Based on a large number of simulations, this methodology allows to identify the most appropriate network configuration(s), which is compatible with the required measurement uncertainty and cost.

The proposed methodology was automated through an ad hoc routine, developed in Matlab®, which makes it possible to simulate the performance of a number of possible network configurations and construct tables and charts, which help in identifying the most convenient one(s). Furthermore, simulations allow to estimate the coverage level of a network and, consequently, to avoid adopting configurations with poor coverage.

The mathematical model for localization is based on the GLS method and is well suited to multi-sensor networks, i.e., networks in which devices of different nature can coexist.

Through some experiments carried out at Politecnico di Torino—DIGEP, we checked the plausibility of the results of the methodology, for a specific distributed LVM system with two types of photogrammetric cameras. These experiments confirmed the feasibility and practicality of the proposed methodology.

The methodology has some limitations, summarized as follows:

- It requires several characteristic data relating to network devices (e.g., uncertainty in angular measurements, range of measurement, location/orientation uncertainty, etc.), which – if not available – should be determined experimentally by ad hoc tests.
- The methodology cannot be applied to multi-sensor networks with more than two types of devices and/or devices able to perform distance measurements.
- The mathematical model used for localization weights the uncertainty contributions from the different network devices, taking into account (i) their uncertainty in angular measurements and (ii) the relative position/orientation of these devices with respect to the target; however, the model does not take into account the uncertainty in their location/orientation.

Future research is aimed at generalizing the proposed methodology, in order to extend it to LVM distributed systems with network devices able to perform both angular and distance measurements. Also, we plan to improve the methodology, in order to simulate the network calibration and determine the uncertainties in the location/orientation of network devices through appropriate simulations, with no more need to estimate them empirically.

Appendix A.

See Table A.1.

Please cite this article in press as: Maisano D, Mastrogiacomo L. A new methodology to design multi-sensor networks for distributed large-volume metrology systems based on triangulation. Precis Eng (2015), http://dx.doi.org/10.1016/j.precisioneng.2015.07.001

Table A.1
Results of the simulations relating to the application example. Configurations are arranged in (descending) lexicographic order with respect to δ and p_A, respectively. The configurations highlighted in grey are characterized by a relatively low coverage (i.e., $Cvg < 95\%$).

Config. no.	δ [m^{-2}]	s [m]	p [%]	c [€/m^2]	Cvg [%]	μ_d [mm]	σ_d [mm]	μ_P [mm]	σ_P [mm]
1	1.78	0.75	22.5	195.1	100.0	0.00	1.18	1.15	0.92
2	1.78	0.75	20.0	181.3	100.0	0.00	1.26	1.22	0.92
3	1.78	0.75	17.5	167.6	100.0	−0.01	1.36	1.32	0.99
4	1.78	0.75	15.0	153.8	100.0	−0.02	1.45	1.43	1.10
5	1.78	0.75	12.5	140.0	100.0	−0.02	1.75	1.59	1.33
6	1.78	0.75	10.0	126.2	100.0	0.00	1.85	1.78	1.47
7	1.78	0.75	7.5	112.4	100.0	0.03	2.22	2.08	1.70
8	1.78	0.75	5.0	98.7	100.0	0.04	2.55	2.51	1.99
9	1.78	0.75	2.5	84.9	100.0	0.04	3.25	3.22	2.36
10	1.78	0.75	0.0	71.1	100.0	0.14	4.64	4.76	3.10
11	1.00	1.00	22.5	109.8	100.0	0.01	1.89	1.67	1.59
12	1.00	1.00	20.0	102.0	100.0	0.01	1.98	1.76	1.62
13	1.00	1.00	17.5	94.3	100.0	0.03	2.21	1.93	1.81
14	1.00	1.00	15.0	86.5	100.0	0.01	2.46	2.14	2.04
15	1.00	1.00	12.5	78.8	100.0	0.03	2.64	2.41	2.23
16	1.00	1.00	10.0	71.0	100.0	0.02	2.94	2.67	2.40
17	1.00	1.00	7.5	63.3	100.0	0.00	3.32	3.14	2.73
18	1.00	1.00	5.0	55.5	100.0	0.03	3.98	3.78	3.10
19	1.00	1.00	2.5	47.8	100.0	0.09	4.76	4.79	3.53
20	1.00	1.00	0.0	40.0	100.0	0.14	6.07	6.40	4.08
21	0.64	1.25	22.5	70.2	99.5	0.05	3.13	2.39	2.88
22	0.64	1.25	20.0	65.3	99.6	0.01	3.05	2.63	2.99
23	0.64	1.25	17.5	60.3	99.6	0.01	3.55	2.79	3.16
24	0.64	1.25	15.0	55.4	99.6	0.00	3.75	3.15	3.50
25	0.64	1.25	12.5	50.4	99.6	0.02	4.03	3.46	3.47
26	0.64	1.25	10.0	45.4	99.7	0.06	4.64	3.92	3.98
27	0.64	1.25	7.5	40.5	99.6	0.07	5.19	4.50	4.20
28	0.64	1.25	5.0	35.5	99.7	0.08	5.76	5.39	4.65
29	0.64	1.25	2.5	30.6	99.8	0.11	6.64	6.58	4.85
30	0.64	1.25	0.0	25.6	99.7	0.13	7.82	8.13	5.20
31	0.44	1.50	22.5	48.8	97.1	0.04	4.32	3.25	3.87
32	0.44	1.50	20.0	45.3	97.2	0.04	4.56	3.51	4.03
33	0.44	1.50	17.5	41.9	97.4	0.02	4.80	3.81	4.30
34	0.44	1.50	15.0	38.4	97.6	0.04	5.22	4.30	4.76
35	0.44	1.50	12.5	35.0	97.6	0.00	5.28	4.80	4.99
36	0.44	1.50	10.0	31.6	97.5	0.06	5.93	5.32	5.12
37	0.44	1.50	7.5	28.1	97.7	0.02	6.60	6.09	5.45
38	0.44	1.50	5.0	24.7	97.9	0.09	7.30	7.14	5.80
39	0.44	1.50	2.5	21.2	97.8	0.09	8.54	8.42	6.18
40	0.44	1.50	0.0	17.8	98.2	0.21	9.47	9.85	6.24
41	0.33	1.75	22.5	35.8	92.7	0.05	5.30	4.32	4.98
42	0.33	1.75	20.0	33.3	92.6	0.07	5.88	4.71	5.51
43	0.33	1.75	17.5	30.8	93.2	0.05	6.22	5.05	5.55
44	0.33	1.75	15.0	28.2	92.8	0.04	6.35	5.52	5.64
45	0.33	1.75	12.5	25.7	93.1	0.11	6.77	6.18	6.10
46	0.33	1.75	10.0	23.2	93.6	0.13	7.69	6.82	6.28
47	0.33	1.75	7.5	20.7	93.6	0.05	8.32	7.78	6.72
48	0.33	1.75	5.0	18.1	94.1	0.09	9.08	8.77	6.99
49	0.33	1.75	2.5	15.6	94.0	0.22	10.08	10.09	7.13
50	0.33	1.75	0.0	13.1	93.9	0.29	11.12	11.63	7.20
51	0.25	2.00	22.5	27.4	86.7	0.06	6.16	5.03	5.91
52	0.25	2.00	20.0	25.5	86.4	0.00	6.83	5.57	6.40
53	0.25	2.00	17.5	23.6	87.1	−0.01	7.08	5.88	6.31
54	0.25	2.00	15.0	21.6	87.5	−0.01	7.67	6.70	6.77
55	0.25	2.00	12.5	19.7	88.0	0.14	8.07	7.28	7.06
56	0.25	2.00	10.0	17.8	87.7	0.12	9.18	8.24	7.46
57	0.25	2.00	7.5	15.8	88.2	0.13	9.35	8.89	7.46
58	0.25	2.00	5.0	13.9	88.3	0.14	10.60	10.35	8.08
59	0.25	2.00	2.5	11.9	88.7	0.26	11.32	11.32	8.06
60	0.25	2.00	0.0	10.0	89.0	0.23	12.46	13.25	8.06
61	0.20	2.25	22.5	21.7	80.9	0.14	7.59	6.19	7.08
62	0.20	2.25	20.0	20.1	81.0	0.03	8.12	6.73	7.33
63	0.20	2.25	17.5	18.6	81.0	0.08	8.74	7.41	7.80
64	0.20	2.25	15.0	17.1	81.7	0.13	9.27	8.03	7.90
65	0.20	2.25	12.5	15.6	81.9	0.16	9.93	8.84	8.22
66	0.20	2.25	10.0	14.0	81.7	0.01	10.54	9.85	8.56
67	0.20	2.25	7.5	12.5	82.3	0.19	11.43	10.92	8.91
68	0.20	2.25	5.0	11.0	82.9	0.26	12.18	12.09	9.04
69	0.20	2.25	2.5	9.4	82.9	0.25	13.19	13.36	9.11
70	0.20	2.25	0.0	7.9	83.0	0.26	14.24	14.97	9.02
71	0.16	2.50	22.5	17.6	74.4	0.10	9.25	7.56	8.30
72	0.16	2.50	20.0	16.3	75.0	0.09	9.31	7.93	8.47
73	0.16	2.50	17.5	15.1	75.4	0.16	9.95	8.84	8.82
74	0.16	2.50	15.0	13.8	76.0	0.17	10.29	9.24	8.77
75	0.16	2.50	12.5	12.6	76.3	0.19	11.30	10.37	9.56

Please cite this article in press as: Maisano D, Mastrogiacomo L. A new methodology to design multi-sensor networks for distributed large-volume metrology systems based on triangulation. Precis Eng (2015), http://dx.doi.org/10.1016/j.precisioneng.2015.07.001

Table A.1 (*Continued*)

76	0.16	2.50	10.0	11.4	76.4	0.09	12.55	11.82	9.75
77	0.16	2.50	7.5	10.1	76.9	0.35	13.31	12.58	10.21
78	0.16	2.50	5.0	8.9	76.9	0.26	13.81	13.96	9.91
79	0.16	2.50	2.5	7.6	78.0	0.37	14.52	14.85	10.03
80	0.16	2.50	0.0	6.4	78.0	0.39	16.00	16.84	9.97
81	0.13	2.75	22.5	14.5	68.6	0.22	10.71	9.12	9.75
82	0.13	2.75	20.0	13.5	68.5	0.16	11.34	9.79	10.04
83	0.13	2.75	17.5	12.5	68.6	0.11	11.73	10.36	10.24
84	0.13	2.75	15.0	11.4	69.5	0.13	12.72	11.59	10.66
85	0.13	2.75	12.5	10.4	69.6	0.11	13.66	12.52	10.99
86	0.13	2.75	10.0	9.4	70.4	0.28	14.28	13.47	11.23
87	0.13	2.75	7.5	8.4	69.9	0.20	14.64	14.21	11.21
88	0.13	2.75	5.0	7.3	71.0	0.42	16.05	16.43	11.51
89	0.13	2.75	2.5	6.3	70.7	0.47	17.22	17.59	11.51
90	0.13	2.75	0.0	5.3	71.0	0.32	17.95	18.96	11.36
91	0.11	3.00	22.5	12.2	63.4	0.09	11.52	9.83	10.33
92	0.11	3.00	20.0	11.3	63.0	0.15	11.72	10.39	10.64
93	0.11	3.00	17.5	10.5	63.7	0.25	12.34	11.11	10.71
94	0.11	3.00	15.0	9.6	64.3	0.18	13.79	12.61	11.26
95	0.11	3.00	12.5	8.7	64.8	0.35	14.49	13.67	11.62
96	0.11	3.00	10.0	7.9	65.1	0.46	14.92	14.47	11.67
97	0.11	3.00	7.5	7.0	65.5	0.32	15.48	15.39	11.88
98	0.11	3.00	5.0	6.2	66.7	0.46	17.40	17.81	11.94
99	0.11	3.00	2.5	5.3	66.5	0.32	18.65	19.06	12.05
100	0.11	3.00	0.0	4.4	66.3	0.60	19.10	20.37	12.05
101	0.09	3.25	22.5	10.4	56.4	0.29	14.04	12.12	12.32
102	0.09	3.25	20.0	9.7	56.7	0.28	14.58	13.02	12.30
103	0.09	3.25	17.5	8.9	56.4	0.20	15.32	13.85	12.66
104	0.09	3.25	15.0	8.2	57.7	0.52	16.12	15.24	13.16
105	0.09	3.25	12.5	7.5	57.7	0.34	16.11	15.11	12.99
106	0.09	3.25	10.0	6.7	58.9	0.21	17.00	16.53	13.32
107	0.09	3.25	7.5	6.0	58.3	0.33	18.24	17.89	13.49
108	0.09	3.25	5.0	5.3	58.7	0.60	19.26	19.43	13.59
109	0.09	3.25	2.5	4.5	59.3	0.64	20.17	20.94	13.44
110	0.09	3.25	0.0	3.8	60.1	0.61	21.41	22.71	13.58
111	0.08	3.50	22.5	9.0	50.8	0.53	14.45	12.64	12.49
112	0.08	3.50	20.0	8.3	51.3	0.39	15.35	13.83	12.85
113	0.08	3.50	17.5	7.7	52.3	0.46	15.90	14.81	13.01
114	0.08	3.50	15.0	7.1	52.5	0.54	17.17	16.18	13.34
115	0.08	3.50	12.5	6.4	53.5	0.33	16.84	15.90	13.24
116	0.08	3.50	10.0	5.8	54.1	0.36	18.00	17.42	13.73
117	0.08	3.50	7.5	5.2	54.1	0.47	18.49	18.80	13.81
118	0.08	3.50	5.0	4.5	54.9	0.58	20.25	20.37	13.77
119	0.08	3.50	2.5	3.9	55.2	0.36	21.21	22.02	13.77
120	0.08	3.50	0.0	3.3	55.7	0.65	22.47	23.82	13.77
121	0.07	3.75	22.5	7.8	45.5	0.38	15.49	13.85	13.35
122	0.07	3.75	20.0	7.3	45.9	0.49	16.24	14.77	13.46
123	0.07	3.75	17.5	6.7	46.7	0.53	17.70	16.31	14.20
124	0.07	3.75	15.0	6.2	47.2	0.53	18.59	17.81	14.54
125	0.07	3.75	12.5	5.6	47.9	0.48	18.34	17.48	14.35
126	0.07	3.75	10.0	5.0	48.4	0.37	19.43	18.69	14.62
127	0.07	3.75	7.5	4.5	48.4	0.63	20.38	20.37	14.75
128	0.07	3.75	5.0	3.9	49.0	0.89	21.31	21.87	14.77
129	0.07	3.75	2.5	3.4	49.6	0.78	22.80	23.90	14.96
130	0.07	3.75	0.0	2.8	50.0	0.78	23.64	25.51	14.60
131	0.06	4.00	22.5	6.9	38.3	0.36	17.64	15.71	15.02
132	0.06	4.00	20.0	6.4	39.3	0.68	18.33	17.04	15.24
133	0.06	4.00	17.5	5.9	39.2	0.67	19.76	18.98	15.54
134	0.06	4.00	15.0	5.4	39.8	0.70	19.62	18.85	15.58
135	0.06	4.00	12.5	4.9	40.9	0.77	21.30	20.73	15.77
136	0.06	4.00	10.0	4.4	41.2	0.47	20.97	20.87	15.82
137	0.06	4.00	7.5	4.0	41.3	0.91	22.30	22.75	15.97
138	0.06	4.00	5.0	3.5	41.7	0.86	24.27	25.16	15.99
139	0.06	4.00	2.5	3.0	42.9	1.01	23.88	25.02	15.83
140	0.06	4.00	0.0	2.5	43.2	1.24	25.53	27.50	15.59

References

[1] Peggs GN, Maropoulos PG, Hughes EB, Forbes AB, Robson S, Ziebart M, et al. Recent developments in large-scale dimensional metrology. Proc Inst Mech Eng B J Eng Manuf 2009;223(6):571–95.
[2] Maropoulos PG, Muelaner JE, Summers MD, Martin OC. A new paradigm in large-scale assembly—research priorities in measurement assisted assembly. Int J Adv Manuf Technol 2014;70(1–4):621–33.
[3] Franceschini F, Maisano D. The evolution of large-scale dimensional metrology from the perspective of scientific articles and patents. Int J Adv Manuf Technol 2014;70(5–8):887–909.
[4] Cuypers W, Van Gestel N, Voet A, Kruth JP, Mingneau J, Bleys P. Optical measurement techniques for mobile and large-scale dimensional metrology. Opt Lasers Eng 2009;47(3–4):292–300.
[5] Franceschini F, Galetto M, Maisano D, Mastrogiacomo L, Pralio B. Distributed large-scale dimensional metrology. London: Springer; 2011.
[6] Muelaner JE, Wang Z, Jamshidi J, Maropoulos PG, Mileham AR, Hughes EB, et al. Study of the uncertainty of angle measurement for a rotary-laser automatic theodolite (R-LAT). Proc Inst Mech Eng B J Eng Manuf 2009;223(3):217–29.
[7] Maisano D, Jamshidi J, Franceschini F, Maropoulos PG, Mastrogiacomo L, Mileham AR, et al. Indoor GPS: system functionality and initial performance evaluation. Int J Manuf Res 2008;3(3):335–49.

Please cite this article in press as: Maisano D, Mastrogiacomo L. A new methodology to design multi-sensor networks for distributed large-volume metrology systems based on triangulation. Precis Eng (2015), http://dx.doi.org/10.1016/j.precisioneng.2015.07.001

[8] Franceschini F, Maisano D, Mastrogiacomo L. Cooperative diagnostics for distributed large-scale dimensional metrology systems based on triangulation. Proc Inst Mech Eng B J Eng Manuf 2013;228(4):479–92.
[9] Bai O, Franceschini F, Galetto M, Mastrogiacomo L, Maisano D. A comparison of two different approaches to camera calibration in LSDM photogrammetric systems. In: ASME (American Society of Mechanical Engineers) 2014 12th biennial conference on engineering systems design and analysis. 2014.
[10] Hartley R, Zisserman A. Multiple view geometry in computer vision. 2nd ed. Cambridge, UK: Cambridge University; 2003.
[11] Wolberg J. Data analysis using the method of least squares: extracting the most information from experiments. Berlin Heidelberg (Germany): Springer; 2005, ISBN 3-540-25674-1.
[12] Kariya T, Kurata H. Generalized least squares. Chichester, UK: John Wiley & Sons; 2004.
[13] Hall BD. On the propagation of uncertainty in complex-valued quantities. Metrologia 2004;41(3):173.
[14] Ross SM. Introduction to probability and statistics for engineers and scientists. London, UK: Academic Press; 2009.
[15] Triggs B, McLauchlan PF, Hartley RI, Fitzgibbon AW. Bundle adjustment—a modern synthesis. In: Vision algorithms: theory and practice. Berlin Heidelberg (Germany): Springer Berlin Heidelberg; 2000. p. 298–372.
[16] Luhmann T, Robson S, Kyle S, Harley I. Close range photogrammetry principles, methods and applications. Scotland: Whittles; 2006.
[17] Hexagon Metrology. Hexagon Metrology; 2015. ⟨http://www.hexagonmetrology.com/⟩ [accessed 15th February 2015].
[18] JCGM 200:2008. VIM – international vocabulary of metrology – basic and general concepts and associated terms (VIM). Geneva, Switzerland: International Organization for Standardization; 2008.

Please cite this article in press as: Maisano D, Mastrogiacomo L. A new methodology to design multi-sensor networks for distributed large-volume metrology systems based on triangulation. Precis Eng (2015), http://dx.doi.org/10.1016/j.precisioneng.2015.07.001